

Preparation, Characterization and Electrochemical Performance of Silicon Coated Natural Graphite as Anode for Lithium Ion Batteries

Mi Lu^{1,*}, Yanyan Tian², Xiaodong Zheng¹, Jun Gao², Bing Huang¹

¹ Clean Energy Research and Development Center, Department of Chemistry and Chemical Engineering, Binzhou University, Binzhou, China, 256603

² Department of Chemistry, Xiamen University, Xiamen, China, 361005

*E-mail: lumihit@sina.com

Received: 28 May 2012 / Accepted: 15 June 2012 / Published: 1 July 2012

The natural graphite (NG) coated silica is prepared by the hydrolysis of tetraethyl silicate, then reduced by magnesium at 700 °C to form NG-Si composite with 10 wt.% silicon. The result of scanning electron microscopy shows that the silicon is coated on the surface of natural graphite with an inhomogeneous distribution. The result of X-ray diffraction shows that the silicon is formed with residual SiO and SiO₂, and the particle size calculated from the Si(111) face is 39.2 nm. The composite with PVdF as binder shows a reversible capacity of 458.8 mAh g⁻¹ with good capacity retention of 85.4% after 50 cycles. The replacement of PVdF by SBR-CMC further improves the capacity retention to 90.7% and the cell charged at 1 C and 2 C rates shows little difference to that charged at 0.1 C. The small particle size is the reason of high capacity retention and the naked NG surface supplies the route for the fast electron transfer. The results present that the NG-Si composite prepared by hydrolysis of tetraethyl silicate on NG, then reduced by magnesium is a simple, low price and easily scale-up method improving the electrochemical performance of silicon anode.

Keywords: Lithium ion battery; Anode; Natural graphite; Silicon

1. INTRODUCTION

The functions of the portable electronic devices such as smart phones are expanding to those of computers. The improved functions require more energy to power it, which results in the much reduced working and standby times of the devices. The development of the batteries with higher energy density is the only way to meet the satisfaction of the consumers and is also the base on the developing of more functions for these portable devices. Lithium ion battery is the only

commercialized rechargeable battery used in these mobile devices and its energy density was mainly determined by the energy density of cathode and anode. For the cathode system, the high voltage cathode such as $\text{LiMn}_{0.5}\text{Ni}_{1.5}\text{O}_4$ and the Li-rich layered compounds show significant promise [1]. For the anode system, the silicon has the highest known theoretical capacity of 4200 mAh g^{-1} and is considered as the most ideal anode for lithium ion batteries. But silicon anode encounters the large capacity fading due to pulverization of silicon and loss of electrical contact between the active material and the current collector [2]. Furthermore, the silicon is a semiconductor, which makes its performance at high current density is poor. Various approaches have been carried out to overcome these issues, including decreasing the particle size to nano-size [3-6], forming of thin film [7-9], surface coating [10-12], forming of alloy [13,14] or active/nonactive composite [15-18]. The forming of porous structure of Si coated with silver shows a stable cyclic capacity after 100 cycles [19]. The core-shell structure silicon nanowire exhibits a capacity about 1000 mAh g^{-1} with stable capacity retention [20]. But from the application view, the nanosized or porous structure increases the specific surface area, therefore increasing the irreversible capacity and lowering the volumetric energy density of lithium ion batteries. The thin film Si electrode generally obtains good performance but is difficult to be scaled-up. The addition of too much carbon into the composite improves its cycling stability but decreases the energy density. Thus, the forming of active/Si composite is advantage for the improvement of energy density of lithium ion battery. The natural graphite (NG) shows high electronic conductivity of $6.4\text{--}8.5 \times 10^{-2} \text{ S cm}^{-1}$ [21] and itself is also a potential anode for lithium ion batteries [22]. Thus the coating of silicon on NG will form a NG/Si composite with a higher reversible capacity than NG, an acceptable of electronic conductivity, and cycling stability than silicon due to the mutual compensate of NG and silicon.

2 EXPERIMENTAL PART

2.1 Preparation of NG/Si composite

The silicon content in the NG-Si composite is 10 wt.%. The sample was prepared by the following steps: (1) the tetraethyl silicate and NG powder were dispersed in the alcohol and stirred overnight to adsorb the tetraethyl silicate on the surface of NG; (2) the mixture of water and alcohol with two drops of acetic acid was added to obtain a suspension, then the suspension was stirred until the solvent was fully evaporated. Then the powder was further drying at $100 \text{ }^\circ\text{C}$ for 3 hrs; (3) the mixture after drying was mixed with 1.5 folds stoichiometric magnesium powder and heat-treated at $700 \text{ }^\circ\text{C}$ for 3 hrs under argon atmosphere to reduce the silica to Si; (4) the powder was put into a 10 wt.% HCl solution to dissolve the Mg and MgO, then it was filtered and rinsed by alcohol several times and dried at $60 \text{ }^\circ\text{C}$ in vacuum to obtain the final NG-Si composite.

2.2 Physical characterization

The morphology of the sample was observed using a scanning electron microscope (SEM) (S4800, Hitachi, Japan) operating at 15 kV. The chemical composition was determined by an energy

dispersive X-ray detector (EDX) coupled with a scanning electron microscope. The structure of the samples was measured by X-ray diffraction (XRD) (X'pert PRO, Panalytical, Netherlands) with CuK α radiation ($\lambda=0.15418$ nm) at the region of 10-90 $^\circ$.

The surface chemical composition was measured by X-ray photoelectron spectroscopy (XPS) using a quantum 2000 scanning ESCA microprobe with monochromatic Al K α radiation (1486.6 eV).

2.3 Electrochemical performance test

Two types of binder were adopted in this experiment: polyvinylidene fluoride (PVdF) and styrene butadiene rubber-carboxymethylcellulose (SBR-CMC). The slurries were prepared by ball-milling the corresponding mixtures for 2 hrs. The component using PVdF as binder is 10:10:80 (PVdF:Super P carbon black: active material) together with an adequate amount of N-methyl-2-pyrrolidone (NMP). While the component of the other slurry is 10:10:10:70 (SBR: CMC: Super P carbon black: active material) with adequate amount of water. The slurry was coated onto copper foil with an area of 1 cm 2 and then dried at 100 $^\circ$ C under vacuum being lower than -0.09 for more than 10 hrs to obtain an electrode for measurement. CR2025 coin-type cells were assembled in an argon-filled glove box (Etelux 2000, China) where both moisture and oxygen levels were kept at less than 1 ppm. LiPF $_6$ (1 mol/L) in ethylene carbonate and dimethyl carbonate (EC-DMC, 1:1 v/v) was used as the electrolyte and lithium foil was used as the counter electrode. Charge/discharge cycles were performed using a Neware $^\circledR$ instrument (China) with different C rates (1 C=372 mA g $^{-1}$). The cyclic voltammetry (CV) was tested by CHI604C (Chenhua, China).

3. RESULTS AND DISCUSSION

3.1 Physical characterization

3.1.1 XRD analysis

The XRD patterns of NG and NG-Si composite are shown in Figure 1. It shows a characteristic of highly crystallized graphite [22]. The peaks corresponding to graphite structure are appeared both for the NG and NG-Si samples, but the intensity of the peaks for the NG-Si is lower than that appeared for the pure NG samples. The obvious graphite peaks indicate that the silicon is not totally covered on the surface of NG. The peaks corresponding to silicon is appeared in the NG-Si pattern, indicating that the silica was reduced by magnesium at high temperatures. The peak appears at 28.34 $^\circ$ is ascribed to the (111) face of Si with a full width at half maximum (FWHM) of 0.20 $^\circ$. The particle size of the reduced silicon calculated from Scherrer's equation is 39.2 nm. The particle size of the Si is determined by that of SiO $_2$. The hydrolysis rate of tetraethyl silicate is accelerated by the addition of base or acid. The spherical SiO $_2$ with larger particle size can be obtained by the addition of ammonia [23].

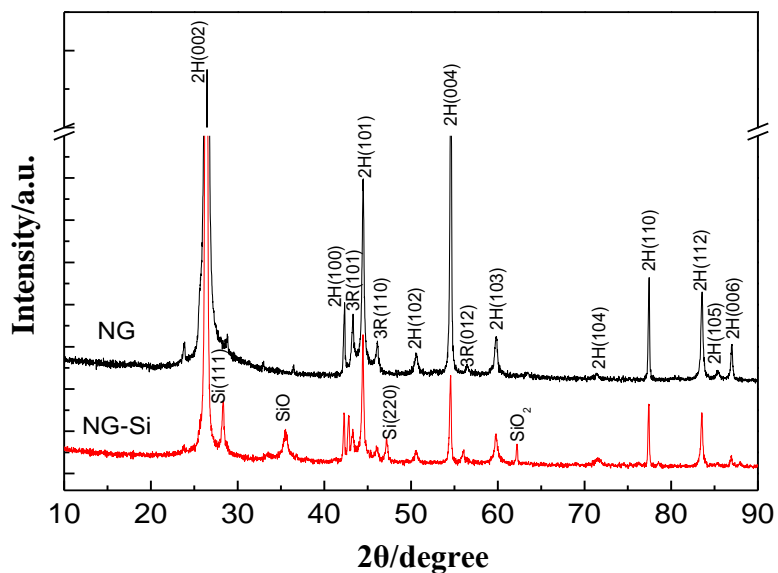


Figure 1. XRD patterns of pure NG and NG-Si composite

3.1.2 SEM and EDX analysis

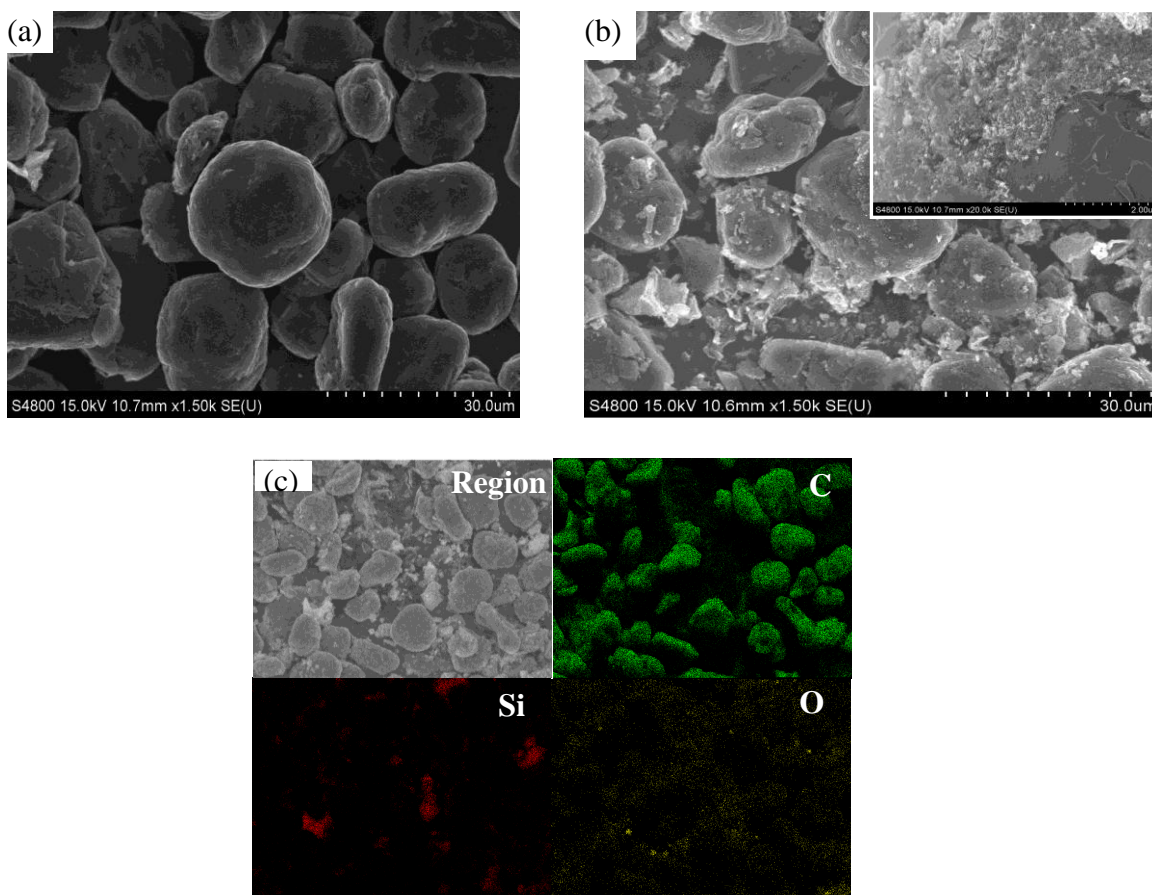


Figure 2. SEM images of pure NG and NG-Si composite. (a) NG; (b) NG-Si; (c) EDX mapping of the NG-Si composite

The SEM of the NG and NG-Si are shown in Figure 2. It shows that pure NG is a spherical morphology. Some of the tinny grains are appeared both on the surface and between the NG powders for the NG-Si sample. The magnified image shows that the silicon is distributed loosely and inhomogeneous on the NG, therefore the signal of graphite is detected in the XRD pattern. The material coated homogeneous silicon can be obtained by the addition of surfactant before the tetraethyl silicate is added [24] or laser-induced vapor deposition [25], but the homogeneous coating of silicon will block the fast transfer route of electrons, therefore decreases the electronic conductivity of Si-NG composite, which will decrease the rate performance of the composite. The EDX of the selected region is shown in Fig.2(c). The results of element distribution show that the carbon is distributed as that appeared in the SEM image, while the silicon is distributed inhomogeneous and the oxygen distribution is like that of the carbon, indicating that the oxygen mainly distributes on the surface of NG.

3.1.3 XPS analysis

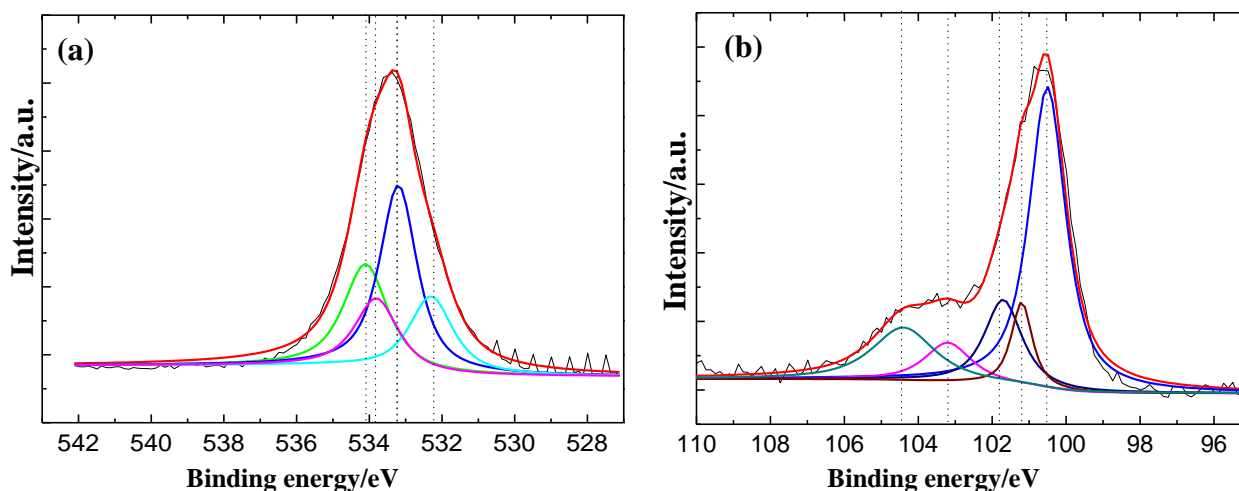


Figure 3. XPS pattern of Ni-Si composite. (a) O1s spectroscopy; (b) Si2p spectroscopy

The O1s and Si2p spectra of NG-Si composite are shown in Figure 3. The O1s spectrum shows that except the peaks at 534.1, 533.2, 532.3 eV corresponding to the oxygen in hydroxyl groups, ether oxygen, carboxylic oxygen in $-\text{COOR}$ ($\text{R}=\text{H}$ and alkyl) [21], respectively, there is a peak at 533.8 eV corresponds to Si-O bond. The much small peak area of Si-O indicates that the oxygen is mainly from the surface functional groups containing oxygen atom of NG, which is bound with the dangling bonds of graphite on the edge face.

The peak at 100.5 eV is ascribed to Si-Si₃ and that at 104.4 eV is unclear yet, but these two bonds are similar to the fluorine plasma-etched silicon surface [26], which shows a much higher binding energy than that of pure silicon (99.4 eV). The peaks at 101.2, 101.7 and 103.2 eV are ascribed

to SiO, SiO_x and SiO₂, respectively [27]. The contents of silicon, SiO₂, SiO_x and Si-O, as calculated from the relative surface area of corresponding peak, are 66%, 9.0%, 11.8% and 13.1%.

3.2 Electrochemical performance of NG and NG-Si anodes with PVdF as binder

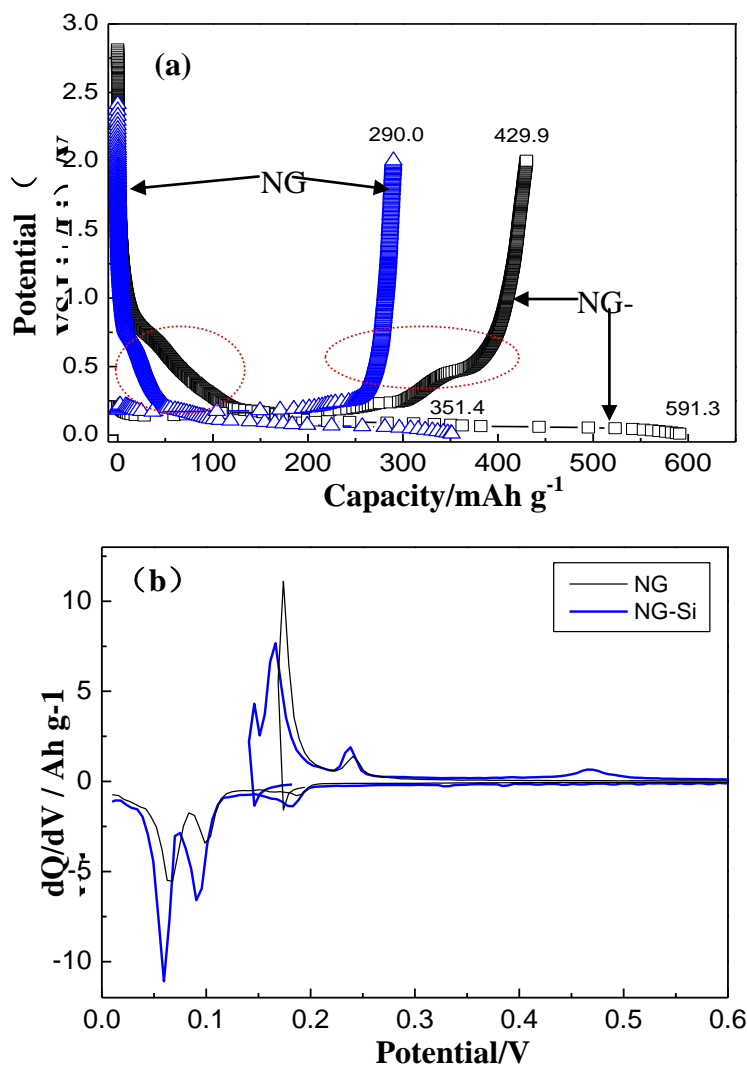


Figure 4. The initial charge-discharge curves of pure NG and NG-Si composite

The cell charge-discharged at 0.1 C and the initial charge-discharged curves are shown in Figure 4. It shows that the pure NG shows a typical charge-discharged characteristic of graphite but changes for the NG-Si sample. The discharged curve of graphite decreases rapidly to below 0.25 V, while that of the NG-Si is decreased gradually, indicating lithium ions begin to insert into the silicon at this potential region; the charged curve of NG-Si shows an obvious plateau appeared at about 0.5V, corresponding to the de-alloying potential of silicon anode. The initial reversible capacities of the NG and NG-Si are different. The de-insertion capacity of pure NG is 290.0 mAh g⁻¹, while that of NG-Si composite is 429.9 mAh g⁻¹, shows a 48.2% higher than that of pure NG and exceeds the theoretical

capacity of graphite (372 mAh g^{-1}). But the coulombic efficiency of NG-Si is about 10% lower than that of pure NG (72.7% vs. 82.5%). The lower coulombic efficiency of NG-Si is ascribed to the small particle size of silicon, resulting in a large surface area of the anode. The increase of capacity and the difference of the charge-discharged curves indicate that the silicon really participates in the reaction and improves the reversible capacity of NG anode.

Figure 3(b) shows the differential capacity curves of NG and NG-Si. On the first discharge, the graphite shows three peaks at 190, 90 and 60 mV are ascribed to the transformation of dilute stage 1 to stage 4, stage 2L to stage 2 and stage 2 to stage 1, respectively. The data are a little lower than that reported (210, 120 and 90 mV, respectively) [28] due to the test is done by a two-electrode system. The peaks of NG-Si begin at about the same potential to that of NG electrode but the peaks are much sharper, indicating that the lithiated capacity at the same potential is larger than that of NG electrode. The peak at about 90 and 55 mV are attributed to the amorphization of crystalline silicon (Li_xSi) and crystalline $\text{Li}_{1.5}\text{Si}_4$, respectively [29]. On the first charge, a small peak corresponding to de-alloying of lithium ions from Li_xSi , the peak are in accordance with the plateau appeared at the charge-discharged curves shown in Figure 3a.

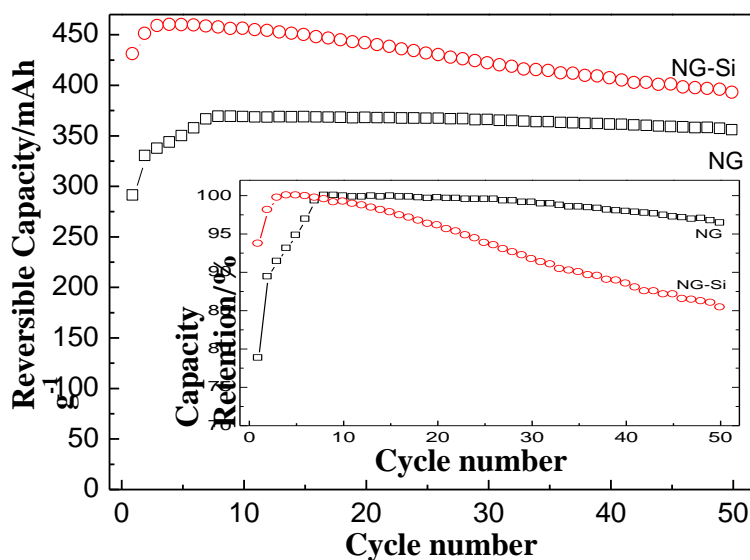


Figure 5. The cycling curves of pure NG and NG-Si composite with PVdF as binder. (The inset plot is the capacity retention of the corresponding samples)

The cycling curves of NG and NG-Si are shown in Figure 5. It shows that the highest irreversible of pure NG is 368.0 mAh g^{-1} , appearing at the 8th cycle; while that of the NG-Si composite is 458.8 mAh g^{-1} , appearing at the 4th cycle. The reversible capacity of pure NG approaches the theoretical capacity of graphite (372 mAh g^{-1}), which is another advantage of NG. The reversible capacity of NG after 50 cycles is 354.7 mAh g^{-1} with a capacity retention is 96.4%; while that of NG-Si composite is 391.7 mAh g^{-1} with lower capacity retention of 85.4%. Results show that the cyclic stability of NG is decreased after silicon coating, but the value is much better than that of the

nanosized Si even with 20 wt.% Super-P carbon black using PVdF as binder [30]. The improved cycling stability is attributed to the small particle size of the silicon on the NG, the NG acts as buffer to reduce the formation of Li-Si alloy with very high lithium content [31], and more importantly, the loose distribution of silicon forms a porous structure, which is a main method improving the cycling stability of silicon electrode [18, 32].

3.3 Electrochemical performance of NG/Si anode with SBR-CMC as binder

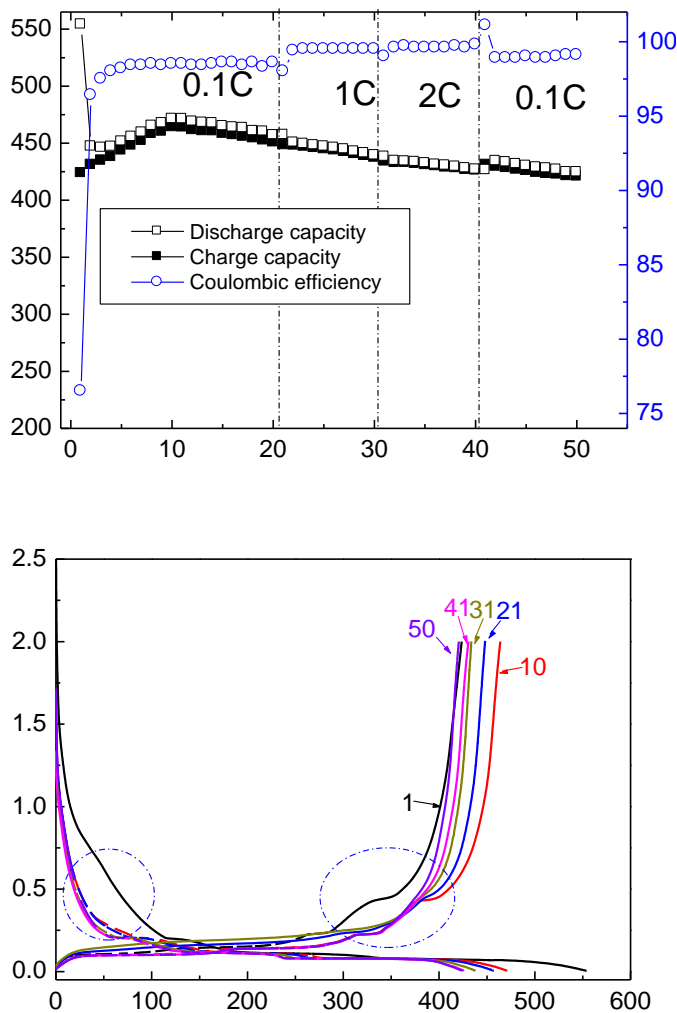


Figure 6. The cycling curves of pure NG and NG-Si composite with SBR-CMC as binder. (a) the cyclic performance; (b) the charge-discharge curves of the selected cycle

For the silicon anode, carboxymethylcellulose (CMC) as binder will significantly improve the stability of silicon anode [33,34]. The reversible capacity of the cell discharged at 0.1 C and charged at 0.1, 1 and 2 C is shown in Figure 6(a). It shows that the cell shows the highest reversible capacity of 464.0 mAh g⁻¹, similar to that with PVdF as binder. The reversible capacity after 50 charge-discharged cycles with different rate is 420.7 mAh g⁻¹, with a capacity retention of 90.7%. Results show that the

replacement of PVdF by SBR-CMC really improves the cycling stability of NG-Si composite. Furthermore, the specific capacity charged at 1 C and 2 C shows little difference to that charged at 0.1C, indicating that the composite shows superior rate performance. The reasons for the improvement of the cycling stability and rate performance may be as follows: the small particle size of the silicon on the NG; the silicon on the surface of NG is inhomogeneous and NG acts as buffer to reduce the formation of high content of Li-Si alloy. The naked surface of NG supplies the route for the fast transfer of the electron, thus the inhomogeneous of silicon coating is advantage for the improvement of the electrochemical performance of NG-Si composite. The coulombic efficiency of the first charged/discharged cycle is 76.5% and reaches higher than 98% after the third charged/discharged cycle.

The charge-discharged curves of the selected cycles are shown in Fig.6(b). It shows that the potential plateau at 0.5 V corresponding to the de-alloying process disappears when the cell charged at 1C, but the potential plateau does not increase much, indicating that the composite shows better rate performance. For the NG-Si composite, the NG is suitable for the SBR-CMC binder, thus the application of SBR-CMC binder for NG-Si composite is no problem.

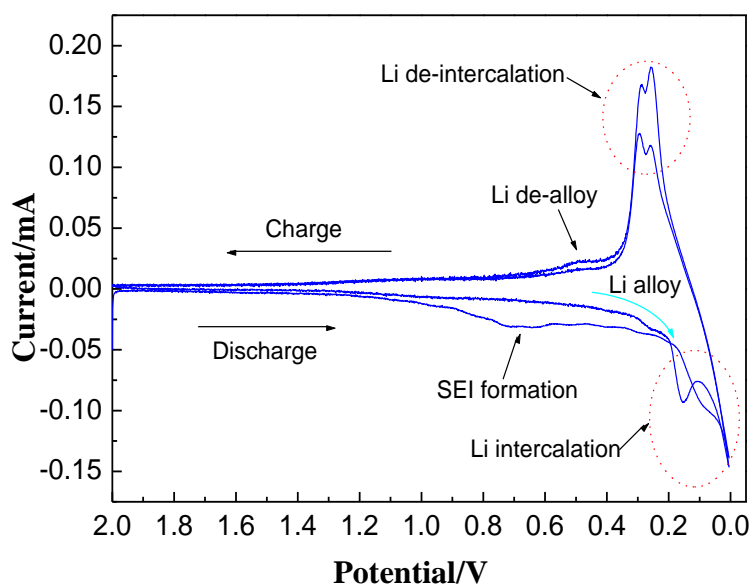


Figure 7. CV curves of NG-Si anode with SBR-CMC as binder

The cyclic voltammetry of NG-Si anode with SBR-CMC as binder is shown in Figure 7. It shows that the current begins to increase below 1.0 V, corresponding to the SEI formation and lithium reacts with silicon, but the current is much reduced during the second cycle. The lithium de-alloying process begins at about 0.5V. The cyclic voltammetry plots are in agreement with the charge-discharged curves shown in Figure 6(b).

4. CONCLUSIONS

The composite of NG-Si prepared from the hydrolysis of tetraethyl silicate to form SiO₂, then reduced by magnesium at 700 °C shows compatibility with PVdF and CMC-SBR binders. The electrode prepared with PVdF as binder shows a reversible capacity and capacity retention after 50 charge/discharged cycles of 458.8 mAh g⁻¹ and 85.4%, respectively; while that with CMC-SBR as binder are 464.0 mAh g⁻¹ and 90.4%, respectively. The NG-Si composite also shows good rate performance. The improved performance is ascribed to the small particle size, the loose and porous structure of the silicon thus prepared, and the inhomogeneous coating of silicon on the surface of NG.

ACKNOWLEDGEMENT

The financial support from the National Natural Science Foundation of China (No. 20903014), Doctoral Fund of Shandong Province (No. BS2010CL001) and Binzhou University (No. 2008Y01, No. 2008ZDL04) is greatly appreciated.

References

1. R. Marom, S. F. Amalraj, N. Leifer, D. J. and D. Aurbach, *J. Mater. Chem.*, 21 (2011) 9938
2. B. Scrosati, J. Garche, *J. Power Sources*, 195 (2010) 2419
3. X. Wang, Z. Wen, Y. Liu, L. Huang, M. Wu, *J. Alloys Compd.*, 506 (2010) 317
4. X.-L. Wang and W.-Q. Han, *ACS Appl. Mater. & Interfaces*, 2 (2010) 3709
5. R. Teki, M. K. Datta, R. Krishnan, T. C. Parker, T.-M. Lu, P. N. Kumta, and N. Koratkar, *Small*, 5 (2009) 2236
6. U. Kasavajjula, C. Wang, A. J. Appleby, *J. Power Sources*, 163 (2007) 1003
7. C.-M. Hwang, C.-H. Lim, J.-W. Park, *Thin Solid Films*, 519 (2011) 2332
8. L. B. Chen, J. Y. Xie, H. C. Yu, T. H. Wang, *Electrochim. Acta*, 53 (2008) 8149
9. T. Zhang, H.P. Zhang, L.C. Yang, B. Wang, Y.P. Wu, T. Takamura. *Electrochim. Acta*, 53 (2008) 5660
10. N. Dimov, S. Kugino, M. Yoshio, *Electrochim. Acta*, 48 (2003) 1579
11. V. A. Sethuraman, K. Kowolik, V. Srinivasan, *J. Power Sources*, 196 (2011) 393
12. H. Ng, J. Wang, D. Wexler, S. Y. Chew, and H. K. Liu, *J. Phys. Chem. C*, 111 (2007) 11131
13. W. Zhou, S. Upreti, M. S. Whittingham, *Electrochem. Comm.*, 13 (2011) 158
14. P. Zuo, G. Yin, Y. Tong, *Solid State Ionics*, 177 (2006) 3297
15. W. Wang, P. N. Kumta, *ACS Nano*, 4 (2010) 2233
16. X. Wang, Z. Wen, Y. Liu, Y. Huang, T.-L. Wen, *Solid State Ionics*, 192 (2011) 330
17. S.Y. Chew, Z.P. Guo, J.Z. Wang, J. Chen, P. Munroe, S.H. Ng, L. Zhao, H.K. Liu, *Electrochem. Comm.*, 9 (2007) 941
18. Y. Zheng, J. Yang, J. Wang, Y. NuLi, *Electrochim. Acta*, 52 (2007) 5863
19. Y. Yu, L. Gu, C. Zhu, S. Tsukimoto, P. A. van Aken, and J. Maier, *Adv. Mater.*, 22 (2010) 2247
20. L.-F. Cui, Y. Yang, C.-M. Hsu, and Y. Cui, *Nano Lett.* 9 (2009) 3370
21. W.Jiang, Solid carbon raw materials, in: W.Jiang (Eds.), Carbon Technology, Metallurgical Industry Press, 2009, pp: 94-115 (In Chinese)
22. M. Lu, Y. Tian, B. Huang, X. Zheng, *J. New Mat. Electrochem. Systems*, 14 (2011) 153
23. T. Zhang, Q. Zhang, J. Ge, J. Goebel, M. Sun, Y. Yan, Y. Liu, C. Chang, J. Guo, Y. Yin, *J. Phys. Chem., C* 113(2009) 3168
24. T.Seeger, Ph. Redlich, N. Grobert, M.Terrones, D.R.M. Walton, H.W.Kroto and M.Rühle, *Chem.Phys.Lett.*, 339 (2001) 41

25. T. Zhang, J. Gao, L. J. Fu, L. C. Yang, Y. P. Wu and H. Q. Wu, *J. Mater. Chem.*, 17 (2007) 1321
26. P. Brault, P. Ranson, H. Estrade-Szwarczopf, B. Rousseau, *J. Appl. Phys.*, 68 (1990) 1702
27. J.-W. Song, C. C. Nguyen and S.-W. Song, *RSC Advances*, 2(2012) 2003
28. Z. Ogumi and M. Inaba, in *Advances in Lithium-Ion Batteries* (W.A. Schalkwijk and B. Scrosati eds.), Kluwer Academic/Plenum Publishers, 2002, New York, 79-102
29. C. Du, M. Chen, L. Wang and G. Yin, *J. Mater. Chem.*, 2011, 21, 15692
30. X. Zhou, Y.-X. Yin, Li.-J. Wan and Y.-G. Guo. *Chem. Comm.*, 48 (2012) 2198
31. X.-Q. Yang, J. McBreen, W.-S. Yoon, M. Yoshio, H. Wang, K. Fukuda, T. Umeno, *Electrochem. Comm.*, 4 (2002) 893
32. M. Chen, C. Du, L. Wang, G. Yin, P. Shi, *Int. J. Electrochem. Sci.*, 7 (2012) 819
33. N. Dimov, H. Noguchi, M. Yoshio, *J. Power Sources*, 156 (2006) 567
34. B. Key, R. Bhattacharyya, M. Morcrette, V. Seznéc, J.-M. Tarascon, and C. P. Grey, *J. Am. Chem. Soc.*, 131(2009) 9239